The discrete complex wavelet approach to phase assignment and a new test bed for related methods

Maria Teodora Ferreira, Celso Bernardo Nóbrega Freitas, Margarete O. Domingues, and Elbert E. N. Macau

Citation: Chaos: An Interdisciplinary Journal of Nonlinear Science **25**, 013117 (2015); doi: 10.1063/1.4906814
View online: http://dx.doi.org/10.1063/1.4906814
View Table of Contents: http://scitation.aip.org/content/aip/journal/chaos/25/1?ver=pdfcov
Published by the AIP Publishing

The discrete complex wavelet approach to phase assignment and a new test bed for related methods

Maria Teodora Ferreira,[a] Celso Bernardo Nóbrega Freitas,[b] Margarete O. Domingues,[c] and Elbert E. N. Macau[d]
Laboratory of Computing and Applied Mathematics - LAC, Brazilian National Institute for Space Research - INPE, São José dos Campos, Brazil

(Received 26 August 2014; accepted 15 January 2015; published online 26 January 2015)

A new approach based on the dual-tree complex wavelet transform is introduced for phase assignment to non-linear oscillators, namely, the *Discrete Complex Wavelet Approach—DCWA*. This methodology is able to measure phase difference with enough accuracy to track fine variations, even in the presence of Gaussian observational noise and when only a single scalar measure of the oscillator is available. So, it can be an especially interesting tool to deal with experimental data. In order to compare it with other phase detection techniques, a testbed is introduced. This testbed provides time series from dynamics similar to non-linear oscillators, such that a theoretical phase choice is known in advance. Moreover, it allows to tune different types of phase synchronization to test phase detection methods under a variety of scenarios. Through numerical benchmarks, we report that the proposed approach is a reliable alternative and that it is particularly effective compared with other methodologies in the presence of moderate to large noises. © *2015 AIP Publishing LLC*.
[http://dx.doi.org/10.1063/1.4906814]

In the context of interacting non-linear oscillators, phase synchronization is a remarkable phenomenon in which a certain relation between phases appears, while their amplitudes can remain with no significant correlation.[1–4] So, investigating phase synchronization requires a clear choice of phase variables, in order to test, for example, if the condition[5] $\Delta\phi(t) = |\phi_2(t) - \phi_1(t)| <$ constant, where $\phi_1(t)$ and $\phi_2(t)$ are the phases of two systems. Therefore, the process of assigning a phase variable to empirical data, also known as phase detection, is the first step required to reveal a myriad of phase synchronization configurations. This process has been fundamental for instance to study ecological systems,[6] coupled neurons,[7,8] geophysical phenomena,[9] chemical oscillators,[10] lasers,[11] plasma physics,[12,13] and biomedical systems.[14–19]

I. INTRODUCTION

For periodic oscillators, one can easily define its phase by taking a variable parameterizing the motion along the limit cycle, with growth proportional to time. Nevertheless, the concept of phase for oscillatory systems is not unique, in the sense that any choice which corresponds to an increment of 2π at each cycle of the phenomenon in the time-scale that one wishes to analyze is equally valid. See Ref. 20 for further discussions about multi-scale synchronization.

In a more general case, involving chaotic systems, for example, phase assignment can be a nontrivial task. Thus, tests of the phase synchronization between systems normally avoid instantaneous phase measurement of the involved signals. Instead, average estimations are considered along well-defined temporal or spatial landmarks, or even statistical measures are applied to certain time windows. These are the cases of the following approaches: Poincaré surface of section,[21] recurrence plots,[22,23] localized sets,[24] and phase diffusion coefficient comparison.[25] These techniques, we should emphasize, are effective in providing indications of phase synchronization in the context of the specific situations for which they were designed. Even so, there are several scenarios for which these methods fail to provide an appropriate response, as will be shown with a variety of numerical experiment in this work. One of these situations is when it is necessary to follow over time instantaneous changes in the phase relationship between the systems, especially in the presence of noise. For example, there are technological applications in which information is embedded in the phase difference between systems evolution,[26] or if one is interested in following the interaction delay between systems.[27]

If one assigns phases via linear interpolation between arrival times of the trajectory in a Poincaré section, by construction, this function will be monotonously increasing with time. However, the phase may loose its physical meaning with this imposition. Some epochs of orientation changes are typically expected,[28] mainly if one considers noise and/or interacting oscillators.[5,29] So, we stress that all methods tested in this work allow increasing or decreasing phase values.

In order to choose a phase variable for a non-linear oscillator, one can use, in principle, direct measurements of phase angles on a attractor projection, as well as more sophisticated techniques such as: Hilbert transform,[1,8] Poincaré surface of section, curvature and recurrence plots,[22,23] localized sets,[24] phase estimation by means of frequency method,[30,31] short-time Fourier transforms, and Continuous

[a]Electronic address: mteodoraf25@gmail.com
[b]Electronic address: cbnfreitas@gmail.com
[c]Electronic address: margarete.domingues@inpe.br
[d]Electronic address: elbert.macau@inpe.br

Complex Wavelet Transform (CWT) methodologies.[32–41] In particular, CWT approaches rely on the complex Morlet wavelet to perform phase detection in chaotic time series, yielding good results for coherent systems.[34,38] So, although it has a high computational cost and may present some interpretation difficulties when applied to large time series, CWT strategies are considered one of the best among the known methods.[8,42]

Aiming to address this shortcoming of the CWT, we propose a new method to phase assignment, the *Discrete Complex Wavelet Approach—DCWA*, based on the Dual-Tree Complex Wavelet Transform (DT–CWT) to pointwise phase assignment. The DT–CWT is a transform that employs two real Discrete Wavelet Transforms (DWTs). The main qualities of this transform are that it is nearly shift invariant, limited redundancy, and reduced computational cost.[43–49]

To allow comparisons among different phase detection methodologies, an innovative testbed is also introduced here. We tailored special orbits with non-linear chaotic oscillators characteristics, such that a theoretical phase choice is known *a priori*. This framework was adopted, instead of classical chaotic oscillators like Rössler or Lorenz, to avoid the usage of a canonical method to obtain a reliable phase choice for comparison purposes. As so, we consider first a Kuramoto model with three interconnected oscillators. Empirically choosing their parameters and the interconnect topology, it is possible to simultaneously produce specific synchronization regimes over each pair of oscillators, ranging from unsynchronized to synchronized, with or without phase slips. Then, the phase signals generated for each oscillator in this Kuramoto model is projected into a surface. We refer this type of coordinate transformation as *embedding*. Our more directed accuracy indicator will be the correct detection in the signal, after this transformation, of phase-slips. Three embedding are considered in this paper to emulate different types and properties of non-linear oscillators: with periodic, coherent and non-coherent orbits. Different intensities of Gaussian observational noise were also added to the data.

Using this testbed, we compare the DCWA with some of the most solid methods in the literature: arctangent method, Hilbert transform, and CWT transform. Besides the advantages of only requiring as input a scalar signal and being robust under moderate noise levels, we point out that our technique has an efficient computational performance when applied to large time series. It is applicable to both phase coherent and non-coherent oscillators. Moreover, it can be successfully applied to non-stationary signals and the choice of parameter values to be used is readily available.

A. Related work

Over time, several methods to phase synchronization detection from experimental measures were introduced.[1,19,22–24,31,34–36,41,50] Also, many other phase detection methods exist in the literature, for example, the synchrosqueezed wavelet transforms[51] (for application, see in Refs. 52–54) which is based on EMD algorithm and the continuous complex wavelet transform. In Ref. 55, it is used protophases for phase extraction from the signal, which utilizes the concepts of the Hilbert and Fourier transform, see Ref. 56. In Ref. 57, the phase description of chaotic oscillators is made by generalizing the concept of standard isophases (isochrones) of periodic oscillators.

There are also measures to test the condition of phase synchronization between systems.[15,19,42,58] For example, in Ref. 19, two synchronization indices are introduced, while in Ref. 15, it is described an application using the mean phase coherence of an angular distribution as a statistical measure. Phase synchronization measures as defined from the Hilbert transform and from the wavelet transform are presented in Ref. 42 and, a method of detecting synchrony in a precise frequency range is shown in Ref. 58. However, to calculate the measures described above, it is first necessary to calculate the phase. Most studies use the Hilbert transform to compute the instantaneous phase (see Refs. 15, 19, 42, and 59) or the continuous complex wavelet transform.[14,42,58–60] As a valuable alternative, we claim that our DCWA for phase assignment can be applied in association with those techniques to obtain more accurate results.

The remainder of this paper is organized as follows. In Sec. II, we present our proposed approach for phase detection. Then, in Sec. III, we construct the testbed to measure the efficiency of the methods. Finally, in Sec. IV, we present results and analysis of our numerical experiments.

II. METHODOLOGY

It is presented in this section our proposed *Discrete Complex Wavelet Approach* (*DCWA*) for phase detection, based on DT–CWT. We begin with a brief description of the DT–CWT and then we follow to our proposed *DCWA* for phase detection. In order to compare our proposed approach, other three traditional methods in the literature for phase assignment are discussed: the arctangent, the Hilbert transform, and the CWT. A description of these methods is include in Appendix A.

A. Dual-tree complex wavelet transform

The DT–CWT is a very carefully constructed transform, from a mathematical and filter bank theory point of view, by Nick Kingsbury in the late 1990s.[44,45,49] We are interested here in the following main features of this quasi-orthogonal complex multi-scale transform: the low computation cost when compared to continuous wavelet transform with Morlet analyzing wavelet, perfect reconstruction with short support filters, good shift invariance, and limited redundancy. More details about these features are discussed in Refs. 43–49.

This is a transform that employs two real DWTs, for details see Appendix B. The first DWT is associated with a filter bank of the upper tree, and it uses low-pass filters $\bar{h}_0$ and high-pass filters $\bar{h}_1$. It computes the multilevel real wavelet coefficients $\bar{d}^j$ that will be used as the real part of the desired complex wavelet coefficients $\boldsymbol{d}^j$. The second DWT is associated with a filter bank of the lower tree, and it is composed of low-pass filters $\underline{h}_0$ and high-pass filters $\underline{h}_1$. Similarly, it computes the $\underline{d}^j$, which contributes to the pure imaginary part of $\boldsymbol{d}^j$. A schematic representation of the DT–CWT decomposition is illustrated in Appendix C.

In this work, we used first scale decomposition (13, 19)-tap-filters, which are bi-orthogonal and near symmetric. For scales $j > 1$, the filters were used Q-Shift filters with (14, 14)-tap-filters.[49] The values for these filters are presented in Appendix D.

B. Discrete complex wavelet approach - DCWA

In order to calculate the phase of an oscillator using our DCWA method, the time series x of oscillator 1, i.e., x_1, is analyzed by the multi-scale DT–CWT. As a result of this transform, we have the time series of the complex wavelet coefficients $\boldsymbol{d}^j$ at each scale j. With these coefficients, the energy E^j at each scale j is calculated as the square of the modulus of complex wavelet coefficients, i.e., $E^j(n) = |\boldsymbol{d}^j(n)|^2$. When, the global wavelet spectrum is computed using $\mathbb{E}^j = \sum_n E^j(n)$. In the next step, the scale J_1 is chosen as the scale of the maximal global energy, i.e., $\mathbb{E}^{J_1} = \max_j \mathbb{E}^j$. Subsequently, the same procedure is applied to the time series x_2 of oscillator 2 and the time series x_3 of oscillator 3. For each oscillator, we have the scale of the maximal global energy J_1, J_2, and J_3. When J_1 was different from J_2 and different from J_3 we chose the scale $J = \min(J_1, J_2, J_3)$. This choice was based on the fact that the number of points N in this multi-scale phase time series is proportional to the scale, i.e., $N = 2^{L-J}$, therefore we chose the larger phase time series. Next, we calculated the phase time series of each oscillator, ϕ_1^J, ϕ_2^J, and ϕ_3^J. The phase ϕ_1^J is calculated from the expression

$$\phi^{J_1}(t) = \mathsf{atan2}(\underline{d}^{J_1}, \bar{d}^{J_1}), \tag{1}$$

wherein $\mathsf{atan2}$ is the arctangent function with two arguments; $\underline{d}^{J_1}$ is the imaginary part of the complex wavelet coefficient in the scale J_1, and $\bar{d}^{J_1}$ is the real part of the complex wavelet coefficient in the scale J_1. The $\mathsf{atan2}$ routine is already built in into many different programming languages. Instead of a single variable, like the standard atan, the former function receives as input two real numbers. Thus, it is possible to correctly choose the quadrant of the computed angle. The phases of the other oscillators are calculated in the same way.

Subsequently, with the objective of verifying the phase synchronization, the combination of the phase difference between them was computed as $\Delta\phi_{12}^J = |\phi_2^J - \phi_1^J|$, $\Delta\phi_{13}^J = |\phi_3^J - \phi_1^J|$, and $\Delta\phi_{23}^J = |\phi_3^J - \phi_2^J|$. Finally, the phase synchronization test condition $\Delta\phi_{12}^J(n) < const < 2\pi$, $\Delta\phi_{13}^J(n) < const < 2\pi$, and $\Delta\phi_{23}^J(n) < const < 2\pi$ is evaluated for each combination.

The phase difference using the phase calculated via our DCWA method considering oscillators 1 and 2 are denoted by $\Delta\phi_{12}^w$; between oscillators 1 and 3 are $\Delta\phi_{13}^w$ and between oscillators 2 and 3 are $\Delta\phi_{23}^w$.

III. THE TESTBED

In this section, we begin with the definition of the Kuramoto Model (KM),[61] which is the core of our testbed. It comprises three not identical Kuramoto oscillators interconnected, so different synchronization regimes between each pairs of oscillators can be obtained by adjusting its parameters. Then, the output signal of the oscillators is transformed through three different embedding. The first one (a) is an embedding from phase variable ϕ into a unit circle in the plane. So, we can illustrate with a simple periodic orbit the usage of the methods. The second one (b) is an embedding from phase variable ϕ to a chaotic curve inside a Möbius strip. Since the Möbius strip has well defined rotation, this embedding plays the role of a coherent attractor. The last one (c) is an embedding from phase variable ϕ to a chaotic curve inside a surface that we call *Double strip*. Since this curve presents larger diffusion coefficient, we may regard it as a non-coherent case. Finally, we explain how the Gaussian observational noise is added to all test sets.

A. Kuramoto model

We assume the following equation for each oscillator $i = 1,\ldots,N$ in KM:

$$\dot{\phi}_i = \omega_i - k\sum_{j=1}^{N} A_{ij}\sin(\phi_i - \phi_j), \tag{2}$$

wherein $\phi_i(t)$ is the phase variable of the *ith* oscillator, assuming values in the real line $\mathbb{R}$, which can also be seen as an angle in the unit circumference, $\phi_i(t) \bmod 2\pi$. The natural frequencies, also known as angular frequencies, of the oscillators are given by the parameters $\omega = (\omega_1, \ldots, \omega_N) \in \mathbb{R}^N$. The constant $k \in \mathbb{R}$ is the coupling strength, which adjusts the intensity of the influence between neighbor oscillators. The coupling graph, which can be direct of undirected, is expressed by its adjacency matrix $A_{N\times N} \doteq (A_{ij})$, with $A_{ii} = 0$; $A_{ij} = 1$, if oscillator i is influenced by oscillator j; and $A_{ij} = 0$, otherwise.

It is chosen to our numerical simulation a KM with $N = 3$ oscillators, because we want to show that our discrete complex wavelet approach is able to simultaneously detect fixed phase synchronization and phase slips.[5] We selected a coupling graph with oscillators 1 and 2 mutually coupled and oscillator 3 acting as a forcing to those oscillators, see Figure 1. The natural frequencies and initial conditions are $\omega = (1.00, 1.05, 1.50)$ and $\phi_0 = \left(0, \frac{2\pi}{3}, \frac{4\pi}{3}\right)$, respectively. Thus, the coupling strength $k = 0.475$ was empirically fixed to show those two different types of synchronization regimes.

It is used an Adams-Bashforth-Moulton Method for the numerical integration (see Ref. 62), with fixed step size $h = 0.01$. The final integration interval is $t_f = 2 \cdot h \cdot 2$,[18] but its first half is eliminate as a transient time. For simplicity, we present time variables beginning at instant $t = 0$.

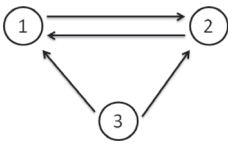

FIG. 1. Schematic representation of the topology connection between oscillators.

B. Kuramoto embeddings

In this subsection, we present the embeddings made in the Kuramoto model and the procedure to add noise.

1. Plane

An embedding in the plan is the simplest, and, this way, we can validate our proposed method with a model that is already described in the variable phase.

To transform the phase variables $\phi \in \mathbb{R}$ of KM (according to Eq. (2)) into the plane $(x, y) \in \mathbb{R}^2$, we simply see ϕ as point in the unit circle with this angle, i.e., we let

$$\begin{aligned} x &= \cos\phi, \\ y &= \sin\phi. \end{aligned} \tag{3}$$

2. Möbius strip

Now, concerning the Möbius strip,[63] the usual parametrization is

$$\begin{aligned} x(u,v) &= \left(1 + \frac{1}{2}\, v \cos\left(\frac{u}{2}\right)\right)\cos u, \\ y(u,v) &= \left(1 + \frac{1}{2}\, v \cos\left(\frac{u}{2}\right)\right)\sin u, \\ z(u,v) &= \frac{1}{2}\, v \sin\left(\frac{u}{2}\right), \end{aligned} \tag{4}$$

wherein $0 \le u \le 2\pi$ and $-1 \le v \le 1$, but we will let $u \in \mathbb{R}$ and set u equal to ϕ from the KM. Figure 2(a) shows schematically two constant lines of this parametrization. Figures 2(b) and 2(c) show one example of this construction increasing the final integration time. Furthermore, we chose v equals to $\cos\tilde{\phi}$, where $\tilde{\phi}$ is an auxiliary oscillator, with $\tilde{\phi}(t) = \tilde{\omega}\, t$, where $\tilde{\omega}$ is an *irrational natural frequency*. So, the orbits defined like this are dense in the Möbius strip, which can be seen as an analogous of the topological transitivity property for chaotic attractors, as discussed in Ref. 64.

We choose irrational natural frequencies for the auxiliary oscillators as $\tilde{\omega} = (\frac{\sqrt{3}}{10}, \frac{\pi}{20}, \frac{\sqrt{2}}{10})$, which is approximately equal to (0.173, 0.157, 0.141) and ten times slower than the oscillators in the direction of u.

3. Double strip

We introduce here a new Kuramoto embedding, the *Double strip*. Roughly speaking, this surface associates an annulus with a Möbius strip in $\mathbb{R}^3$. It was empirically designed to present orbits with higher diffusion constant, which is a feature found, for instance, in the non-coherent Rössler Attractor $\dot{x} = y + z$, $\dot{y} = x + 0.2y$, $\dot{z} = 0.2 + xz - 5.7z$ (for information about non-coherent Rössler Attractor look,[65] and for diffusion constant see Ref. 6).

The position of the oscillator in this figure is defined by a seed $v \in [0, 1]$ and a phase ϕ, so we denote this point by $X(v, \phi)$. Moreover, this map will be defined such that, at every cycle of the oscillator, it returns to a Poincaré Section S given by the line segment joining the origin to $(1, 0, 0)$, more specifically $X(v, 2k\pi) \in S$ for all $k \ge 0$. Thus, we may also define a Poincaré map $P(v_k) = v_{k+1}$ of the successive returns of the orbit to S, since $X(v_k, 2(k+1)\pi) = (v_{k+1}, 0, 0) \in S$.

For a given point in $(v, 0, 0) \in S$, the oscillator will travel in its next cycle $\phi \in [0, 2\pi]$ through a annulus-like surface, that we call *Normal strip*, if $v \in [0, 0.5]$ (as can be seen in Figure 3(a)). Or through a surface similar to a Möbius strip, that we name Inversion strip, if $v \in (0.5, 1]$ (as can be seen in Figure 3(b)). Another property of the map X that will be established by construction is that $P(v) = 2v$, if v belongs to the Normal strip; and $P(v) = -2v + 2$, if v belongs to the Inversion strip (as can be seen in Figure 3(d)). For this reason, we can argue that the dynamics in the Double strip is chaotic, since its Poincaré Map P is the Tent Map, which is a classical chaotic discrete map (for more information see Ref. 66).

The position of the oscillator in the Normal strip is given by $X(v, \phi) = f(v, \phi)$ defined by

$$\begin{aligned} f(v,\phi) &:= (1 - \lambda_f(v))\, v_0(\phi) + \lambda_f(v)\, v_{0.5}(\phi), \\ &\text{for } (v,\phi) \in [0, 0.5] \times \mathbb{R}, \end{aligned} \tag{5}$$

where

$$\begin{aligned} v_0(\phi) &= 0.5(\cos\phi,\ \sin\phi, 0) - (0.5, 0, 0); \\ v_{0.5}(\phi) &= (\phi/(4\pi) + 1)(\cos\phi,\ \sin\phi, 0) - (0.5, 0, 0); \\ \lambda_f(v) &= 2v. \end{aligned} \tag{6}$$

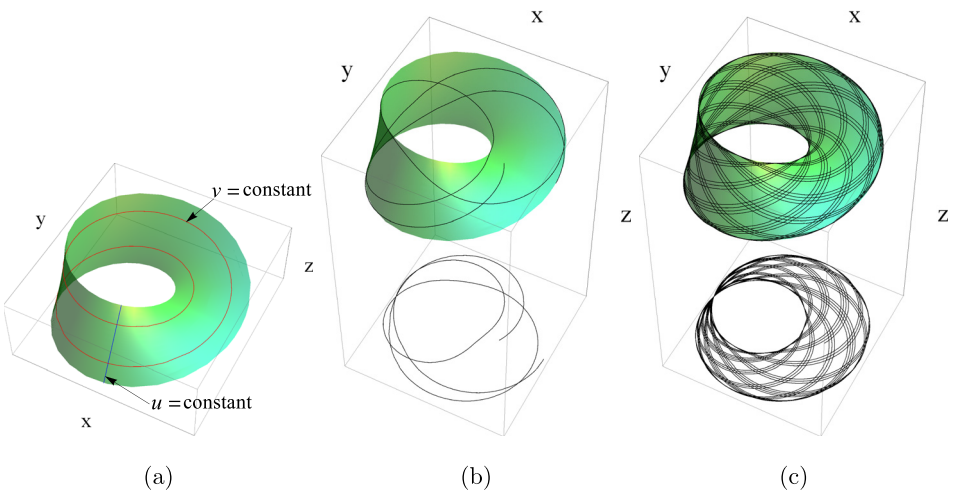

FIG. 2. Möbius strip (a) indicates two curves given by constant lines of its parametrization (according to Eq. (4)); (b) and (c) orbit of an uncoupled oscillator combined with an irrational auxiliary oscillator, with final integration time $t_f = 4\pi$ and $t_f = 40\pi$, respectively. A projection into (x, y) plane is also shown.

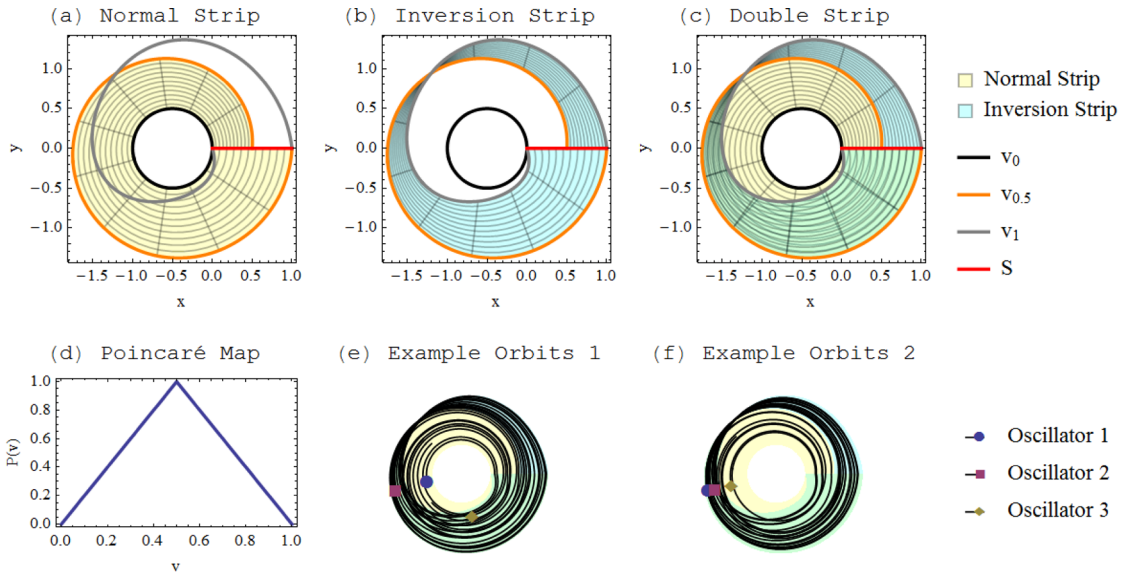

FIG. 3. (a)–(c) Double strip construction scheme. (d) The Poincaré return map considering section S. (e) and (f) Examples of embedded orbits for the Kuramoto model described in Subsection III A. (e) The most common behavior, while (f) display the moment during phase slips when oscillator 3 gives an additional spin and crosses oscillators 1 and 2.

In the other hand, the position of the oscillator in the Inversion strip is given by $X(v,\phi) = g(v,\phi)$ with

$$g(v,\phi) := (1-\lambda_g(v))\, v_{0.5}(\phi) + \lambda_g(v)\, v_{1.0}(\phi), \quad \text{for } (v,\phi) \in (0.5,1] \times \mathbb{R}, \tag{7}$$

wherein

$$\begin{aligned} v_{1.0}(\phi) &= ((1+0.5\gamma(\phi)\cos(\phi/2))\cos\phi - 0.5, \\ &\quad \times (1+0.5\cos(\phi/2))\sin(u), 0.5\sin(\phi/2)); \\ \gamma(v) &= 0.5(v-\pi)^2/\pi^2 + 0.5; \\ \lambda_g(v) &= -1+2v. \end{aligned} \tag{8}$$

Geometrically, the image of X was designed such that $X([0,0.5]\times[0,2\pi])$ interpolates between curves $v_0([0,2\pi])$ and $v_{0.5}([0,2\pi])$, which forms the Normal strip; while $X([0.5,1]\times[0,2\pi])$ interpolates between $v_{0.5}([0,2\pi])$ and $v_1([0,2\pi])$, defining the Inversion strip, see Fig. 3(c). The initial seeds for each of the three oscillators where chosen randomly with uniform distribution over [0, 1].

Figures 3(e) and 3(f) illustrate the Double strip embedding for the Kuramoto model with parameters described in Subsection III A.

4. Applying noise

Through numerical integration, a discrete approximation $\phi(0),\ldots,\phi(t_f)$ for the solution of model (2) is computed, according to Subsection III A. Then, one of the embeddings $F(.)$ is applied, yielding $F(\phi(0)),\ldots,F(\phi(t_f))$. Let X_i denote the time series of the ith coordinates obtained like this, i.e., $X_i := (F(\phi(0))_i,\ldots,F(\phi(t_f))_i)$.

We separately perturb each coordinate with a non-correlated additive noise $X_i + \xi\alpha$, where α is the intensity of the white noise. If $\alpha = 0$, no noise is included. Otherwise, we generate $\xi_\alpha = \alpha\tilde{\sigma}\mathcal{N}$, where $0 \le \alpha \le 1$; $\tilde{\sigma}$ is the standard deviation of X_i; and $\mathcal{N}$ are random numbers chosen from a standard normal distribution. Noise intensities of $\alpha = 0$, 0.10,…, 0.90, 1.0 are explored in this article.

Figures 4(a)–4(c) show the orbits of those three oscillators in the Möbius strip, according to Subsection III A, considering the intensity noise $\alpha = 0$ in (a); (b) $\alpha = 0.10$ and (c) $\alpha = 0.20$.

C. Unwrapping stage

In a first moment, all methods studied here provide wrapped phases, meaning that they are limited to the unit circle $[0, 2\pi)$. Thus, to quantity how many cycles one oscillator overtakes another, we must apply an unwrapping stage. This procedure accumulates the phase difference between consecutive discrete times, with a threshold difference of π to distinguish between phase increments and phase decrements. Thus, it is clearly necessary a sufficiently small discretization time. Otherwise, successive phase differences may become larger than π not because a phase decrement, but due to its fast dynamics in comparison with the sampling rate. Since our fastest uncouple oscillator evolves 0.015 rad per time step (see Sec. III A), in general, this assumption is easily satisfied.

IV. RESULTS

We present now the results of the phase difference assignment considering the Kuramoto model embedding in the plane, in the Möbius strip, and in the Double strip. The theoretical phase difference between oscillators i and j, from the Kuramoto model itself, is denoted by $\Delta\phi_{ij}^{k}$. The phase difference assigned by the arctangent method, Hilbert transform, the CWT and our DCWA method are denoted by $\Delta\phi_{ij}^{t}$, $\Delta\phi_{ij}^{hilbert}$, $\Delta\phi_{ij}^{cwt}$, and $\Delta\phi_{ij}^{w}$, respectively.

We stress that no preliminary filter or denoising procedure is applied before using any of the methods studied.

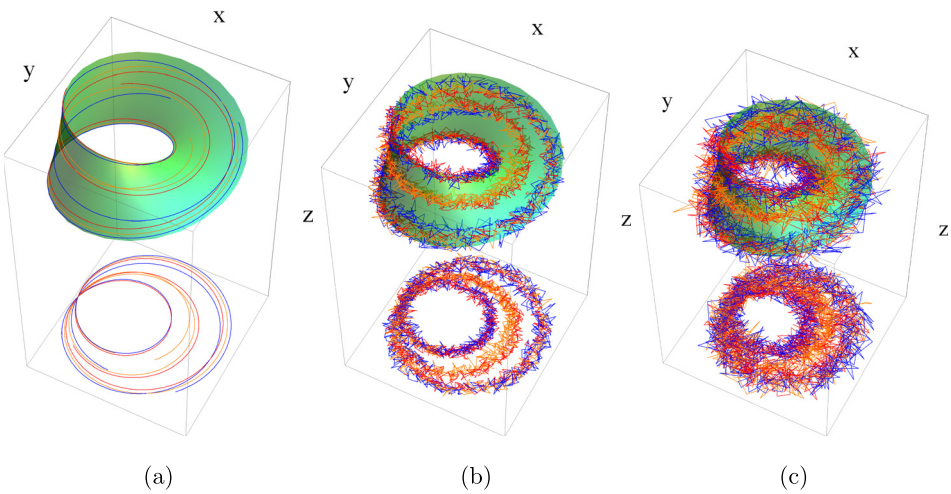

FIG. 4. (a)–(c) Illustrate the orbit of oscillators in the Möbius strip with oscillator 1 in blue, 2 in orange, and 3 in red as described in Subsection III A, considering the intensity noise in (a) $\alpha = 0$, (b) $\alpha = 0.10$, and (c) $\alpha = 0.20$. Projections into (x, y) plane are also shown.

Besides, an unwrapping process to transform consecutive phase points from the unit circle [0, 2?) into continuous real values, adding 2π every complete cycle, is applied in all methods according to Sec. III C.

A. Kuramoto model in the plane

We discuss now the results for the Kuramoto model embedded in the plane.

In this case, were found very small values of diffusion coefficient, describing a system with coherent phase, as discussed in Ref. 6. The values for each oscillator are $\tilde{D}_1 = 0.049659$, $\tilde{D}_2 = 0.11847$, and $\tilde{D}_3 = 0.01476$. The average diffusion coefficient is $\tilde{D}_{average} = 0.060963$.

Figure 5 displays (a) the global wavelet spectrum of the Kuramoto model in the plane considering $\alpha = 0$. The phase difference between oscillators of the Kuramoto model in the plane without noise ($\alpha = 0$) using (b) the theoretical KM, (c) arctangent method, (d) Hilbert transform, (e) the CWT transform, and (f) our DCWA method.

Note that, for oscillators 1 and 2, the scale of maximum energy is $J = 9$ and for oscillator 3, the scale of maximum energy is $J = 8$, as can be seen in Fig. 5(a). Here, we consider the scale $J = 9$ in the phase difference assignment. The scale $J = 8$ was also tested and showed similar results when used to scale $J = 9$ and, for this reason, there is illustrated here. When we consider the presence of noise, the global wavelet spectrum shows the same scale of maximum energy found when $\alpha = 0$ and, therefore is not illustrated here.

Note in Figure 5 that all methods were able to verify phase synchronization between oscillators 1 and 2, as well as the phase slips between oscillators 1 and 3 and oscillators 2 and 3. Note that applying CWT, as can be seen in Fig. 5(e), the detection of phase slips were not as expected given by theoretical KM, as can be seen in Fig. 5(b).

Considering the presence of noise $\alpha = 0.10$, $\alpha = 0.20$, and $\alpha = 0.30$, the results are similar for the three tested methods, arctangent method, Hilbert transform, and our DCWA method, were able to reconstruct the original phase difference of the Kuramoto model. Figure 6 shows the phase difference between oscillators of the Kuramoto model in the plane, with the intensity of noisy $\alpha = 0.30$ considering in (a) the theoretical KM, (b) arctangent method, (c) Hilbert transform, and (d) our DCWA method.

Observed from Figure 6 that even with an intensity of noise $\alpha = 0.30$, the three methods were able to reconstruct the original phase difference of the Kuramoto model. Oscillators 1 and 2 are phase synchronized, since their phase difference is almost zero. Oscillator 3 presents phase slips relative to oscillators 1 and 2: for approximately every 500 time units, oscillator 3 gives one additional spin around oscillators 1 and 2, almost like a jump, and then returns to an almost constant phase difference. An important feature was that our discrete complex wavelet approach was much less sensitive to the noise than the arctangent method and Hilbert transform.

However, for further increments in the noise level ($\alpha = 0.40$), the arctangent method and the Hilbert transform fail to correctly identify phase slips and phase synchronization, as can be seen in Figures 7(b) and 7(c).

Figure 7 shows the phase difference between oscillators, of the Kuramoto model in the plane, with the intensity of noisy $\alpha = 0.40$ considering in (a) the theoretical KM, (b) arctangent method, (c) Hilbert transform, and (d) our DCWA method.

Analysing the results obtained from arctangent method, Figure 7(b), three false phase slips are detected between oscillators 1 and 2, in the interval $t \approx 640$, $t \approx 860$, and $t \approx 1950$. Considering the oscillators 1 and 3 three false phase slips are detected in the interval $t \approx 640$, $t \approx 790$, and $t \approx 885$; and between oscillators 2 and 3 four false phase slips are detected in the interval $t \approx 790$, $t \approx 860$, $t \approx 885$, and $t \approx 1950$.

Note in Figure 7(c), the Hilbert transform fail to correctly identify phase slips and phase synchronization. When we consider the phase difference between oscillators 1 and 2, the Hilbert transform erroneously detects 12 regions of phase slips. Considering the phase difference between oscillators 1 and 3, are erroneously detected 15 phase slips and when we consider oscillators 2 and 3 are erroneously detected 12 phase slips.

The our DCWA method correctly detect phase slips and phase synchronization, as can be seen in Figure 7(d) and compared with the theoretical KM in Figure 7(a). Even for

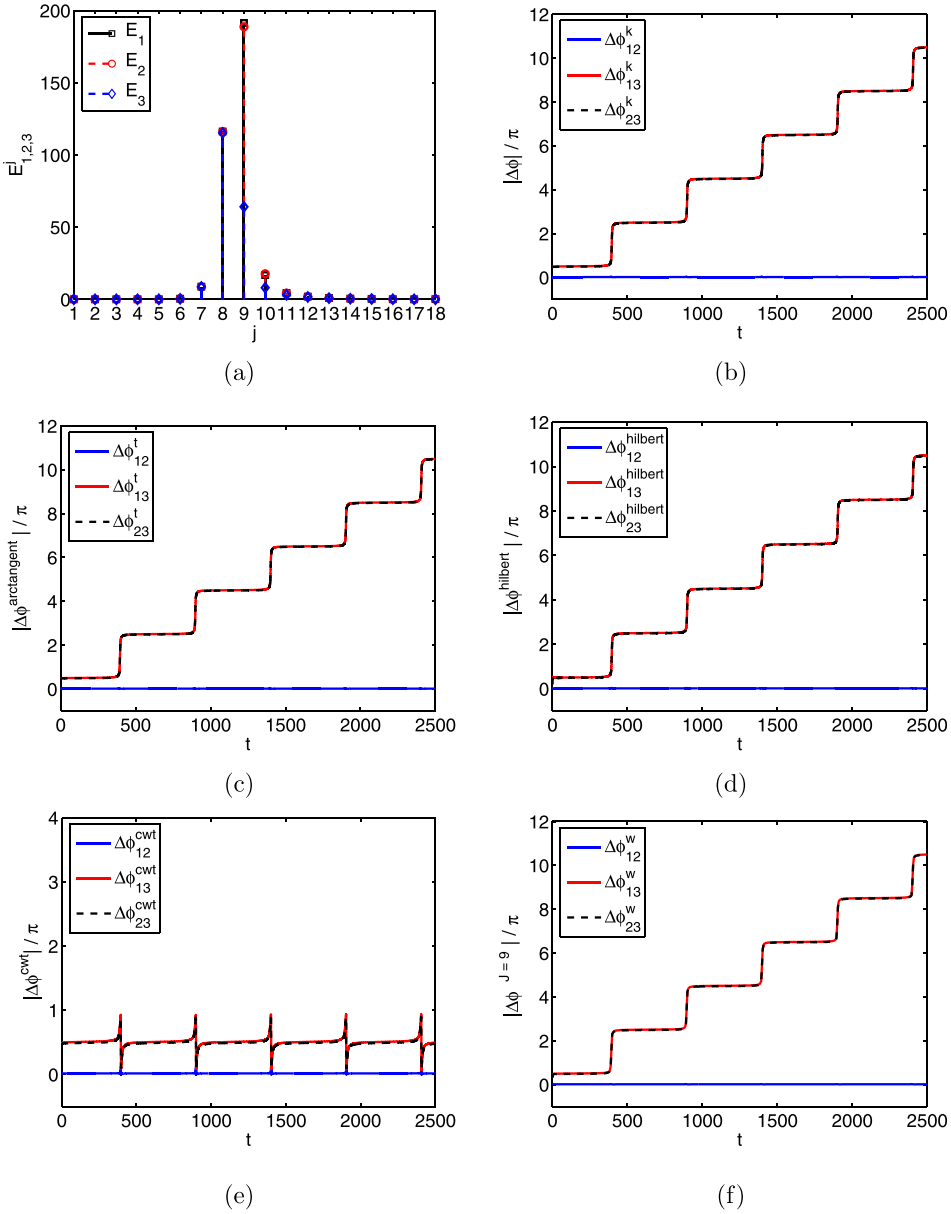

FIG. 5. In (a), the global wavelet spectrum of the Kuramoto model in the plane considering $\alpha = 0$. The phase difference between oscillators when $\alpha = 0$ Kuramoto model plane, considering in (b) the theoretical KM, (c) arctangent method, (d) Hilbert transform, (e) the CWT transform, and (f) our DCWA method.

noise levels up to $\alpha = 2.0$, our DCWA method correctly detect phase slips and phase synchronization, not shown here.

B. Kuramoto model in the Möbius strip

We discuss now the results of the Kuramoto model embedded in a Möbius strip.

In this case, were found small values of diffusion coefficient characterizing a system with coherent phase, as discussed in Ref. 6. The values for each oscillator are $\tilde{D}_1 = 0.18605$, $\tilde{D}_2 = 0.11314$, and $\tilde{D}_3 = 0.013888$. The average diffusion coefficient is $\tilde{D}_{average} = 0.10436$.

Figure 8 displays (a) the global wavelet spectrum of the Kuramoto model in Möbius strip, considering $\alpha = 0$. The phase difference between oscillators of the Kuramoto model in Möbius strip without noise ($\alpha = 0$) using in (b) the theoretical KM, (c) arctangent method, (d) Hilbert transform, (e) the CWT transform, and (f) our DCWA method. Note that, for oscillators 1 and 2, the scale of maximum energy $J = 9$ and for oscillator 3, the scale of maximum energy is $J = 8$, as can be seen in Fig. 8(a). Both results of the global wavelet spectrum are similar with noise, and therefore are not illustrated here. The scale $J = 9$ was used to calculate the phase difference between oscillators. The scale $J = 8$ was also tested and showed similar results when used to scale $J = 9$, and for this reason, there is illustrated here.

Observed from Figures 8(c), 8(d), and 8(f) that the arctangent method, Hilbert transform, and our DCWA method were able to reconstruct the original phase difference of the Kuramoto model (see Figure 8(b)). The CWT transform erroneously detected two phase slips between oscillators 1 and 2. With respect to phase slips occurring between oscillators 1 and 3 and oscillators 2 and 3, the CWT correctly detect the intervals (in time) occurring this phase slips, but do not correctly detect the value thereof, as can be seen in Fig. 8(e).

Despite the fact that our DCWA method presented small perturbations in its results, the method successfully detected the phase slips and phase synchronization. Below, we discuss what can be these perturbations.

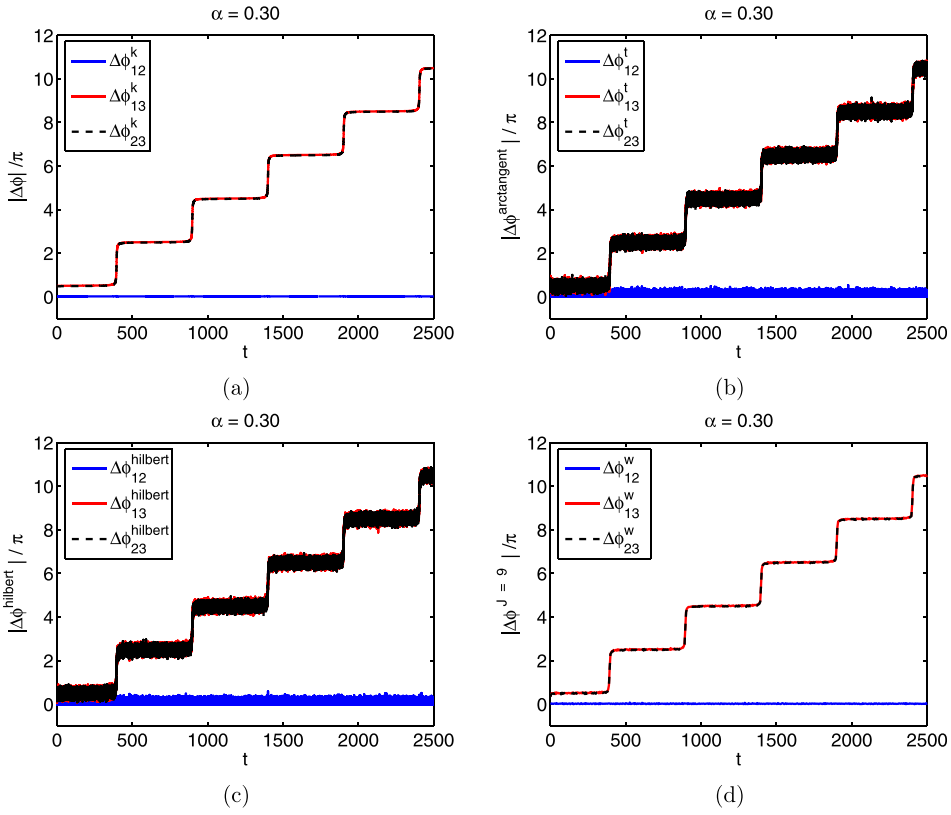

FIG. 6. The phase difference between oscillators, of the Kuramoto model in the plane, with the intensity of noisy $\alpha = 0.30$ considering in (a) the theoretical KM, (b) arctangent method, (c) Hilbert transform, and (d) our DCWA method.

Figure 9(a) displays the zoom of phase difference between oscillators of the Kuramoto model in Möbius strip without noise, $\alpha = 0$, considering our DCWA method. Here, we want to show why the perturbations where found in the phase difference when applied our DCWA method. In Figures 9(b), 9(c), and 9(d), the interval $t = [1350, 1450]$ of the time series of oscillators 1 and 2; 1 and 3; and 2 and 3 are presented, respectively. Note that in Figure 9(a) the phase

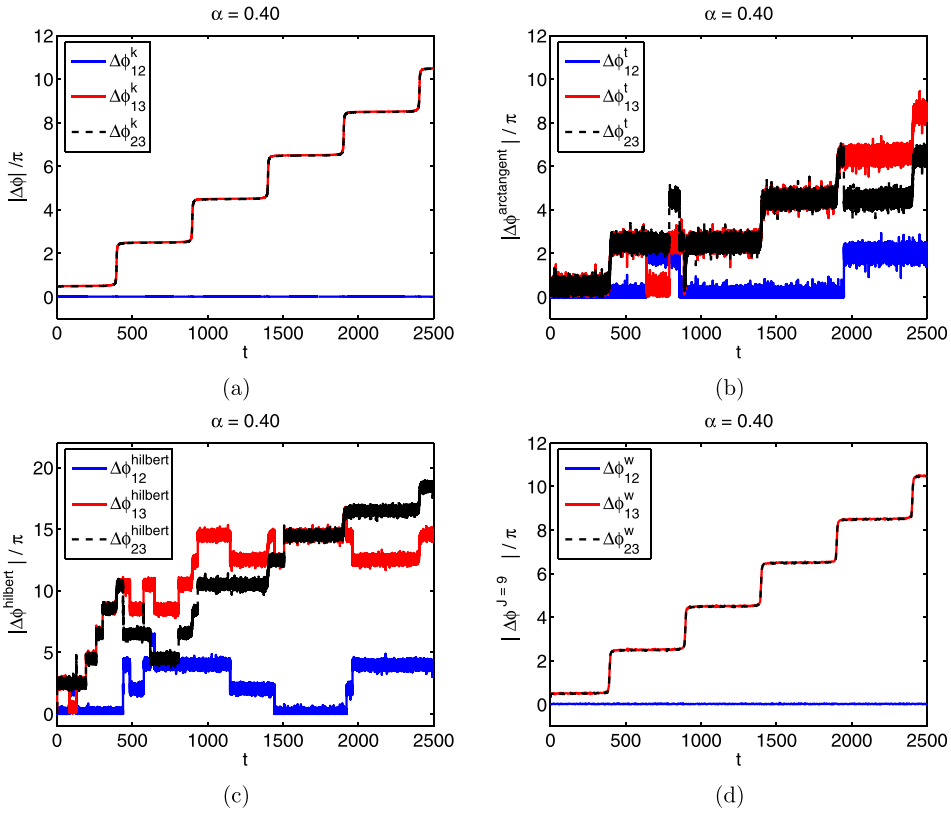

FIG. 7. The phase difference between oscillators, of the Kuramoto model in the plane, with the intensity of noisy $\alpha = 0.40$ considering in (a) the theoretical KM, (b) arctangent method, (c) Hilbert transform, and (d) our DCWA method.

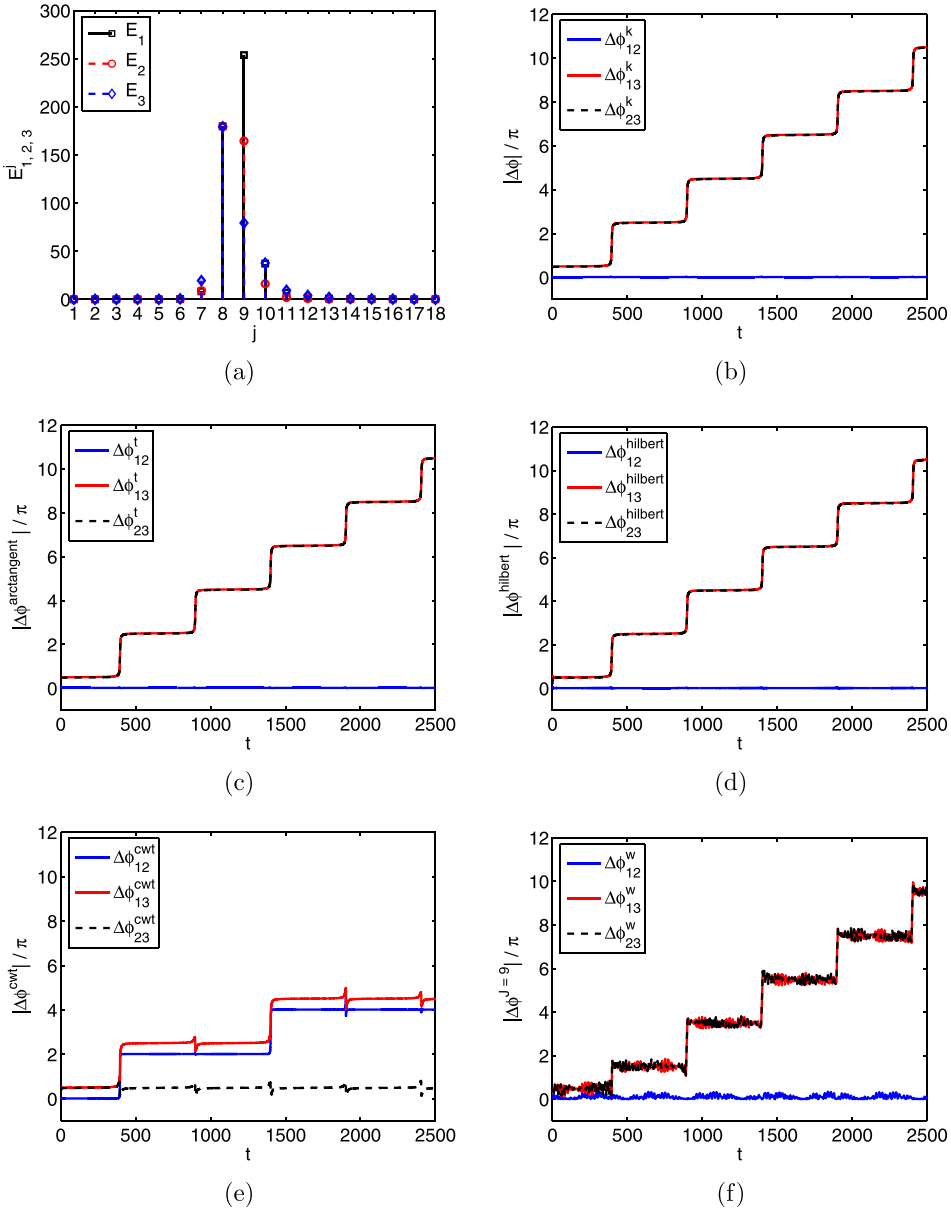

FIG. 8. Results of the Kuramoto model embedded in a Möbius strip. In (a), the global wavelet spectrum and the phase difference between oscillators, considering in (b) the Kuramoto model in the Möbius strip with $\alpha = 0$; (c) arctangent method; (d) Hilbert transform; (e) the CWT transform; and (f) our DCWA method.

difference of oscillators 1 and 2 oscillate around zero and the phase difference of the oscillators 1 and 3 and 2 and 3 oscillate around 3.5 in $t \approx [1350,1390]$. In the interval $t = [1390,1410]$, there is a phase slips between oscillators 1 and 3 and 2 and 3, and the phase difference starts to oscillate around 5.5. Observing this interval of the time series of oscillators (see Figures 9(b)–9(d)), we note that the method was able to associate the oscillations found in the phase difference with their delays and/or advances present in time series of oscillators. Note that the other methods were not able to verify this phenomenon, being this one of characteristic of the proposed method.

Considering the presence of noise $\alpha = 0.10$ and $\alpha = 0.20$, the results are similar for the three methods, arctangent method, Hilbert transform, and our DCWA method, were able to reconstruct the original phase difference of the Kuramoto model.

Figure 10 shows the phase difference between oscillators, of the Kuramoto model in Möbius strip, with the intensity of noisy $\alpha = 0.20$ considering in (a) the theoretical KM, (b) arctangent method, (c) Hilbert transform, and (d) our DCWA method.

Fig. 10 shows that the three methods were able to detect phase synchronization, like in the previous experiment without noise (Figure 8). However, the Hilbert transform erroneously detects a region of the phase slip between oscillators 1 and 3 and oscillators 2 and 3 in the interval $t \approx 490$ (see Figure 10(c)). Nevertheless, our DCWA method was again much less sensitive to the noise than the arctangent method and Hilbert transform.

Increasing the amount of noise for $\alpha = 0.30$, the arctangent method and the Hilbert transform fail to correctly identify phase slips and phase synchronization, as can be seen in Figures 11(b) and 11(c). In this case, these methods detect various phase slips which verifying in the evolution of the time series, the same does not occur. However, the our DCWA method correctly detects phase slips and phase synchronization, as can be seen in Figure 11(d).

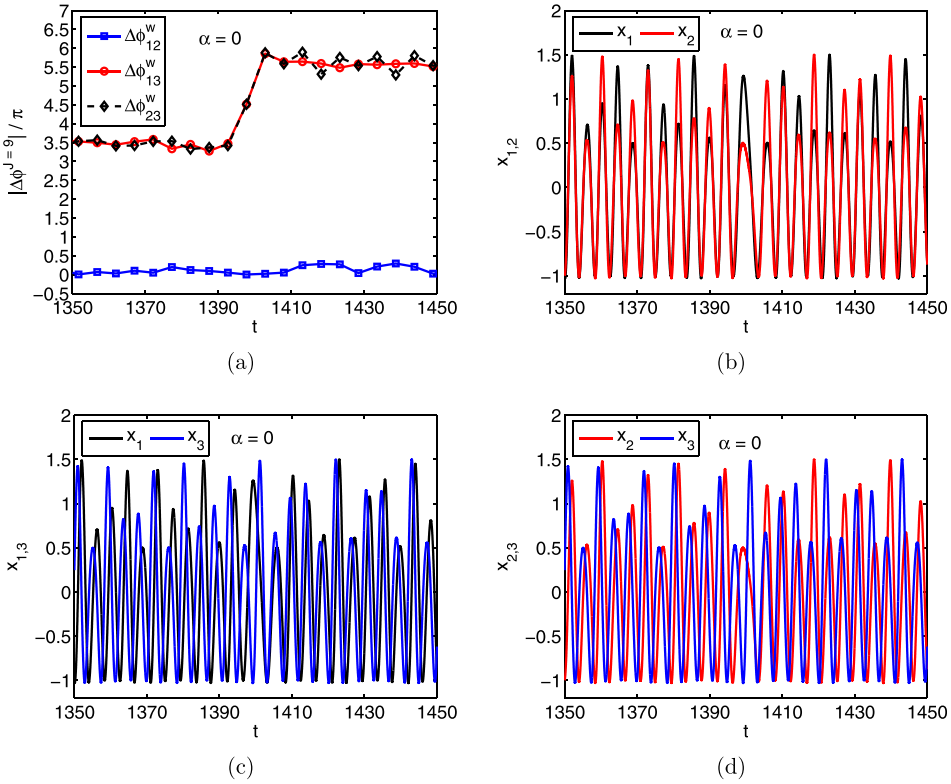

FIG. 9. In (a), the zoom of phase difference between oscillators when $\alpha = 0$ considering our DCWA method and the interval $t = [1350, 1450]$ of the time series of the oscillators in (b) 1 and 2; (c) 1 and 3, (d) 2 and 3.

Figure 11 shows the phase difference between oscillators of the Kuramoto model in a Möbius strip, with intensity of noise $\alpha = 0.30$, considering in (a) the theoretical KM, (b) arctangent method, (c) Hilbert transform, and (d) our DCWA method.

Beyond this level of noise $\alpha = 0.30$, our DCWA method does not detect correctly phase slips and phase synchronization only for $\alpha = 1.6$, not shown here.

C. Kuramoto model in the Double strip

We discuss now the results of the Kuramoto model embedded in a Double strip.

In this case, higher values of diffusion coefficient were found, characterizing a system with more non-coherent phase, as discussed in Ref. 6, The values for each oscillator

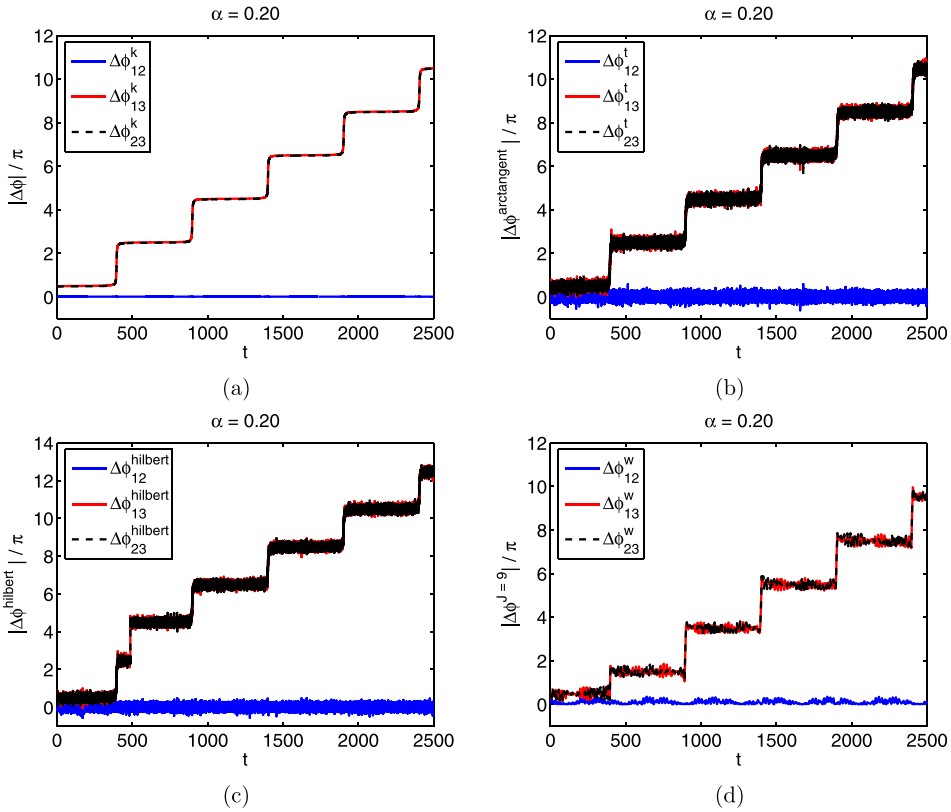

FIG. 10. The phase difference between oscillators, of the Kuramoto model in Möbius strip, with intensity of noise $\alpha = 0.20$, considering in (a) the theoretical KM, (b) arctangent method, (c) Hilbert transform, and (d) our DCWA method.

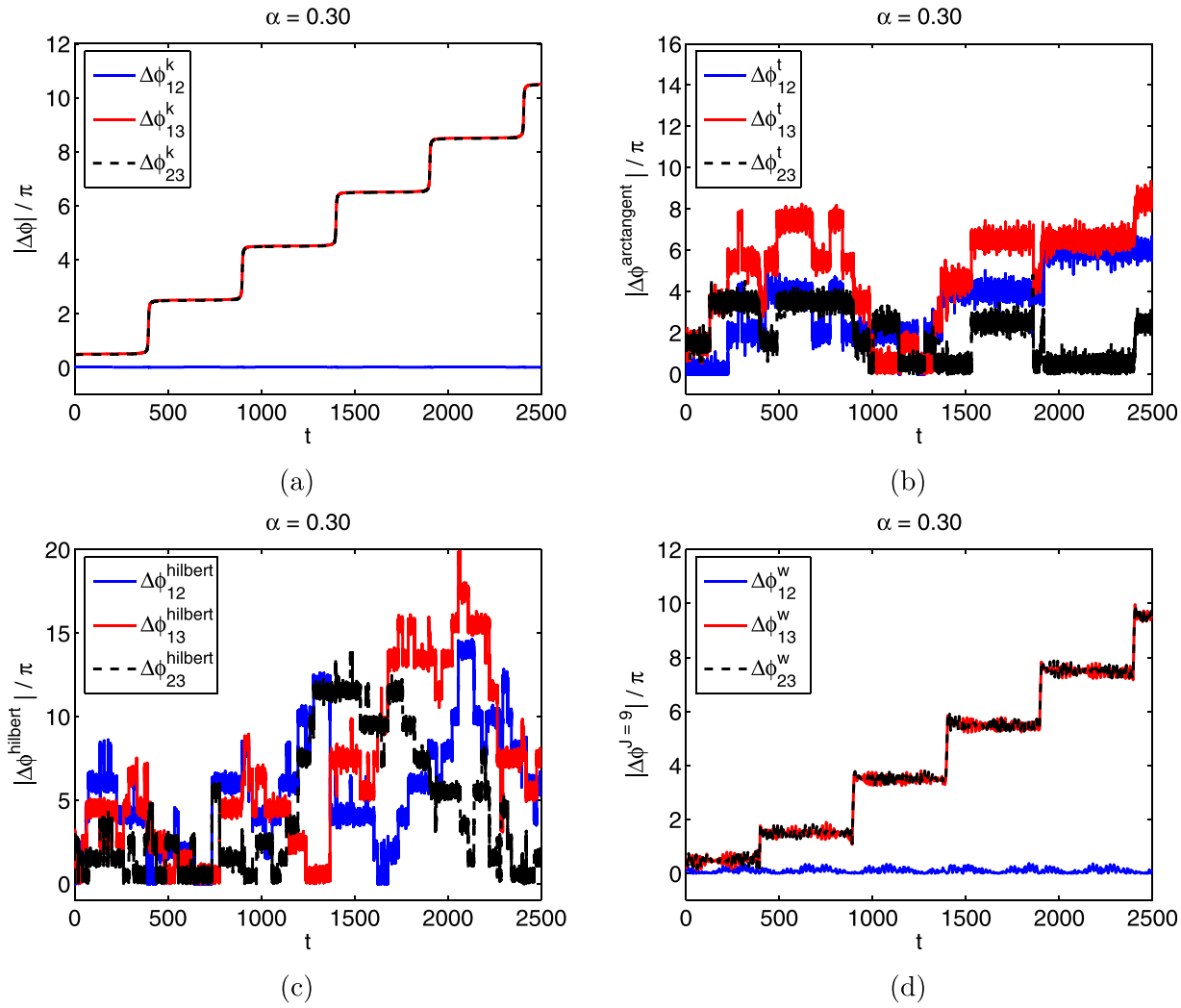

FIG. 11. The phase difference between oscillators, of the Kuramoto model in Möbius strip, with the intensity of noise $\alpha = 0.30$ considering in (a) the theoretical KM, (b) arctangent method, (c) Hilbert transform, and (d) our DCWA method.

are $\tilde{D}_1 = 0.0894731$, $\tilde{D}_2 = 0.159167$, and $\tilde{D}_3 = 0.11774$. The average diffusion coefficient is $\tilde{D}_{average} = 0.12213$.

Figure 12 shows (a) the global wavelet spectrum and the phase difference between oscillators, considering (b) the Kuramoto model in the Double strip without noise ($\alpha = 0$), (c) arctangent method, (d) Hilbert transform, (e) CWT transform, and (f) our DCWA method.

Considering without noise and with the presence of noise, from $\alpha = 0.10$ to $\alpha = 2.0$, the method based on arctangent detects erroneously the phase slips between oscillators 1 and 3 and oscillators 2 and 3 in intervals $t \approx 1550$, $t \approx 1780$, and $t \approx 2210$. The phase slip in intervals $t \approx 1550$ and $t \approx 1780$ are detected erroneously between oscillators 1 and 2.

Considering without noise and with the presence of noise $\alpha = 0.10$ up to $\alpha = 2.0$, the method based Hilbert transform detects erroneously the phase slips between oscillators 1 and 3 and oscillators 2 and 3 in intervals $t \approx 650$, $t \approx 1100$, $t \approx 1550$, $t \approx 1750$, $t \approx 2210$, and $t \approx 2420$. The phase slip in intervals $t \approx 650$, $t \approx 1100$, $t \approx 1550$, $t \approx 1750$, and $t \approx 2420$ are detected erroneously between oscillators 1 and 2.

Applying the CWT, considering without noise, the phase slip in intervals $t \approx 1400$ and $t \approx 2400$, are detected erroneously between oscillators 1 and 2. Again, the method detects the intervals at which phase slips occur, but does not correctly detect the value of it.

Considering the case without noise and with the presence of noise $\alpha = 0.10$ up to $\alpha = 2.0$, our DCWA method correctly detect the phase slips between oscillators 1 and 3 and oscillators 2 and 3 and the phase synchronization between oscillators 1 and 2.

V. CONCLUSIONS

In this work, we introduced a new approach, based on the DT–CWT, for phase detection. This approach is not just able to measure the phase difference between oscillators, but also presents sensitivity enough to track instantaneous variation in the phase difference between them, even in the presence of noise. The main advantage of our approach is that it can be applied directly to scalar experimental time series. Furthermore, our methodology allows us to work with time series with a large number of points and it presents a low computational cost (order of $2N$, where N is the number of points).

In order to compare different techniques, we also introduced an innovative testbed. Three test sets based on

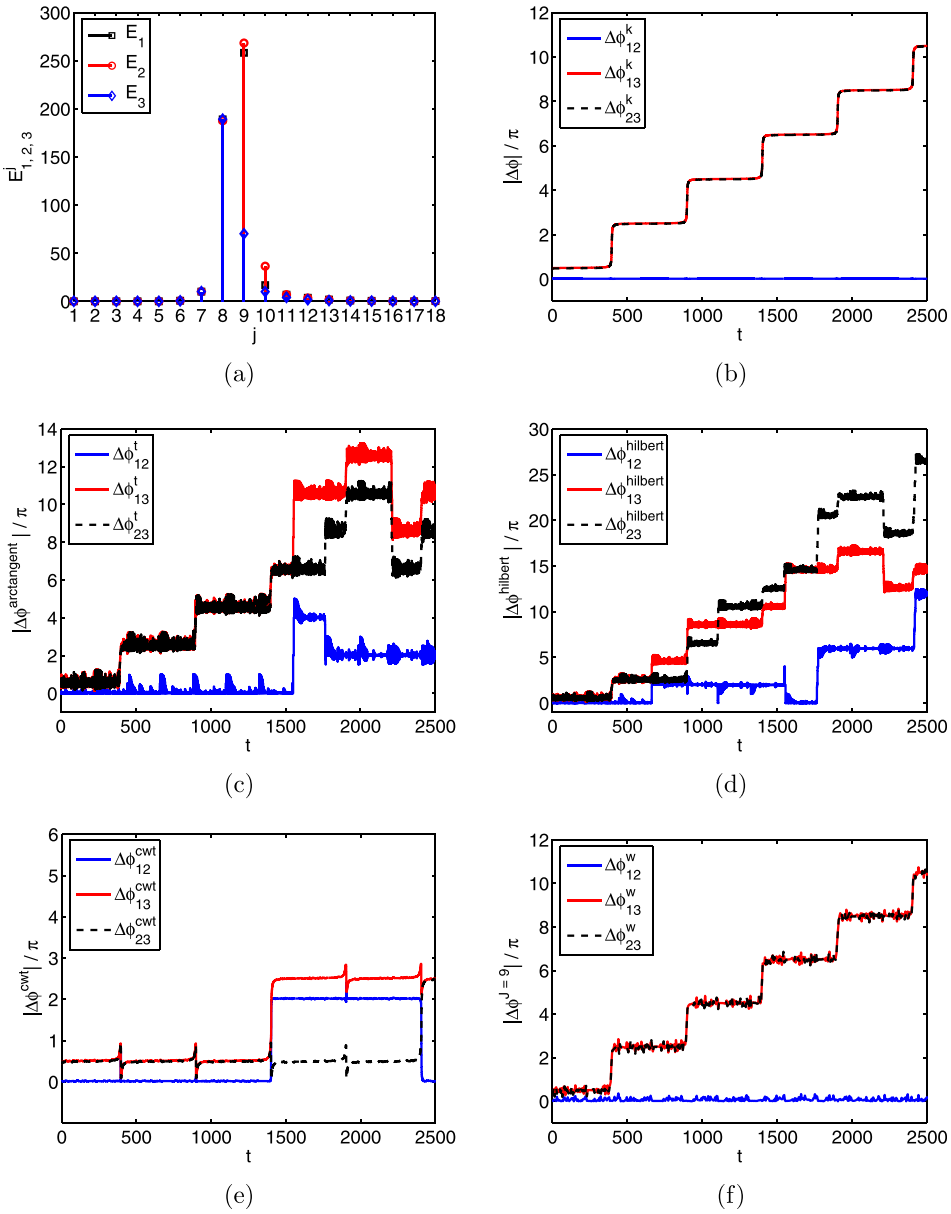

FIG. 12. Results of the Kuramoto model embedded in a Double strip. In (a), the global wavelet spectrum and the phase difference between oscillators, considering in (b) the Kuramoto model in Double strip, without noisy $\alpha = 0$ (c) arctangent method; (d) Hilbert transform; (e) CWT transform; and (f) our DCWA method.

embedding of the Kuramoto model in $\mathbb{R}^3$ were discussed, which are a by-product contribution of this work.

The evaluations reported allow us to claim that our proposed approach, the *Discrete Complex Wavelet Approach—DCWA*, is very effective in accomplish the task for which it was conceived.

The next step in the research will be to extend the method to enable the analysis of energy over time, as well as other filters in the analysis. The applicability of our proposed method will also be tested in chaotic dynamic systems, such as Rössler and Lorenz systems, and sets of experimental data, possibly under different time-scale synchrony regimes.

ACKNOWLEDGMENTS

This work was supported by CAPES, CNPq (Grant Nos. 309667/2013-5, 306828/2010-3, 483226/2011-4, 10571/13-2, and 304582/2010-7) and FAPESP (Grant No. 2011/50151-0).

Nick Kingsbury for giving the algorithm DT–CWT and presented two mini-courses on this subject in the WWlet/CNMAC 2012.

APPENDIX A: OTHER METHODS

1. Arctagent method

It is the most common method for measuring phase if it is possible to project the underlying attractor on a plane so that the projection looks like a smeared limit cycle[67] with well-defined rotation center.

In this and other similar cases, the phase $\phi(t)$ presents coherent phase and can be measured as the angle in the polar coordinate system on the plane (x, y), as proposed by Ref. 1, as follows:

$$\phi(t) = \arctan\left(\frac{y}{x}\right). \tag{A1}$$

In the case where the system displays non-coherent phase, the phase can be defined using the projection of the attractor on the plane of the derivative, as proposed in Ref. 68 using the equation

$$\phi(t) = \arctan\left(\frac{\dot{y}}{\dot{x}}\right). \tag{A2}$$

Note that, to calculate the phase using these methods it is necessary to know the two state variables, namely, x and y. But, this is not always available.

In this approach, the arctangent function is defined as a four-quadrant operation.

In this work, the phase difference using the phase calculated via the method based on arctangent function considering oscillators 1 and 2 are denoted by $\Delta\phi^{t}_{12}$; between oscillators 1 and 3 are $\Delta\phi^{t}_{13}$ and oscillators 2 and 3 are $\Delta\phi^{t}_{23}$.

2. Hilbert transform

A consistent way to define the phase for an arbitrary signal is known in signal processing as the analytic signal concept.[5] This general approach, based on the Hilbert transform (HT), unambiguously gives the instantaneous phase $\phi(t)$ and amplitude $A(t)$ for a signal $s(t)$ via construction of the analytic signal $\zeta(t)$, which is a complex function of time defined as (for details see Ref. 5)

$$\zeta(t) = s(t) + \imath\, s_H(t) = A(t)\, e^{\imath\,\phi(t)}. \tag{A3}$$

Here, the function $s_H(t)$ is the HT of $s(t)$

$$s_H(t) = \pi^{-1}\, P.V. \int_{-\infty}^{\infty} \frac{s(\tau)}{t-\tau} d\tau \tag{A4}$$

where P.V. means that the integral is taken in the sense of the Cauchy principal value.

In this work, the phase difference using the phase calculated via the method based on Hilbert transform considering oscillators 1 and 2 are denoted by $\Delta\phi^{hilbert}_{12}$; between oscillators 1 and 3 are $\Delta\phi^{hilbert}_{13}$ and oscillators 2 and 3 are $\Delta\phi^{hilbert}_{23}$.

3. Continuous wavelet transform

The CWT is a tool that allows to decompose the time series into different components of frequencies. This transform considers that the translation and scale parameters are continuous, and transforms a one-dimensional time series (time) in a two-dimensional representation (time, scale) that can be highly redundant.

The CWT in $L^2(\mathbb{R})$ of a time series $f(t)$ can be defined as

$$\mathcal{W}^{s}_{n}(t) = \frac{1}{\sqrt{s}} \int_{-\infty}^{\infty} f(t)\, \psi^{*}\left(\frac{t-n}{s}\right) dt, \tag{A5}$$

wherein $s, n \in \mathbb{R}$, $s \neq 0$, * denotes the complex conjugate and the term $\frac{1}{\sqrt{s}}$ is a normalization factor of the signal energy.

The wavelet spectra, also called scalograms, represent the squared amplitudes of the module of wavelet coefficients, which can be interpreted as the distribution of signal energy in time t by its scale.[69]

The global wavelet spectrum is the time integration of scalogram, or

$$S_{\psi}(s) = \int \mathcal{W}^{s}_{n}(s,n)\, dt. \tag{A6}$$

The Morlet wavelet consists of a plane wave modulated by a Gaussian function that is expressed by

$$\psi^{Morlet}(t) = e^{-\imath\,\omega_0\, t}\, e^{-t^2/2}, \tag{A7}$$

wherein ω_0 is a non dimensionless frequency. This wavelet function is a complex function, which allows to analyze the phase and the modulus of the decomposed signal.

In this work, the phase difference using the phase calculated via the method based on CWT considering oscillators 1 and 2 are denoted by $\Delta\phi^{cwt}_{12}$; between oscillators 1 and 3 are $\Delta\phi^{cwt}_{13}$ and oscillators 2 and 3 are $\Delta\phi^{cwt}_{23}$.

APPENDIX B: DISCRETE WAVELET TRANSFORM

The DWT presents four important attractive characteristics, namely, good compression of signal energy, perfect reconstruction with short support filters, no redundancy, and very low computation cost (order N operations).[49] As this transform is a real transform, we cannot use it to compute the phase. However, it will be used here as a tool to compute the DT–CWT.

The DWT is implemented in discrete values of scale j and localization n, and provides a time-scale analysis of any finite energy signal x, where $j, n \in \mathbb{Z}$. Mathematically, the signal x can be decomposed in terms of basis functions, as for instance, the scale function φ. However, we can represent this signal also in a multi-scale way using a multi-resolution analysis (MR) tool.

A MR is constructed by using embedded spaces $V^j \supset V^{j+1}$ that have as basis functions φ^j, which are a Riez basis; the union of these spaces are $L^2(\mathbb{R})$; the intersection of these spaces is zero; their functions have scalability proprieties. The difference between two spaces V^j and V^{j+1} is the detail space, where the wavelet functions are Riesz basis, as described in detail in Refs. 69 and 70. Thus, we can represent x in a multi-scale way considering just one scale function φ and its associated wavelet functions ψ as

$$x(t) = \sum_{n\in\mathbb{Z}} c^{j}_{n}\varphi^{j}_{n}(t) + \sum_{j,n\in\mathbb{Z}} d^{j}_{n}\psi^{j}_{n}(t), \tag{B1}$$

wherein c^{j}_{n} are scale coefficients, $c^{j}_{n} = \int x(t)\, \varphi^{j}_{n}(t)\, dt$, and d^{j}_{n} are wavelet coefficients $d^{j}_{n} = \int x(t)\psi^{j}_{n}(t)\, dt$. These coefficients are calculated by using a very efficient, linear complexity algorithm based on convolutions of the analyzed signal x with a discrete-time low-pass filter h_0 and a high-pass filter h_1 with downsampling operations $\downarrow 2$. This is called the Mallat algorithm or Mallat-tree decomposition[69,70] and it is the DWT. The c^{j}_{n} and d^{j}_{n} are associated to h_0 and h_1. Moreover, they have a scale relation

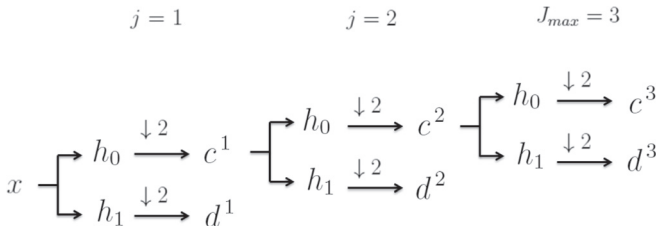

FIG. 13. Scheme of the DWT decomposition of the signal x in three scales, $j=1$, 2 and $j=3$).

$$c_n^j = \sum_{k\in Z} h_0(k)c_{n-k}^{j-1}, \quad d_n^j = \sum_k h_1(k)c_{n-k}^{j-1},$$

where one possibility is to choose $h_1(k) = (-1)^k h_0(1-k)$. Therefore, the following relations can be obtained:

$$\varphi_n^j(t) = \sum_n h_0(n)\varphi_n^{j-1}(t), \quad \psi_n^j(t) = \sum_n h_1(n)\,\varphi_n^{j-1}(t).$$

Figure 13 shows a scheme of the DWT decomposition in three scales of the real signal x. The signal is analyzed independently and simultaneously by using the filters h_0 and h_1 and then decimated by a factor of 2 (denoted as $\downarrow 2$), generating two 1-scale coefficients given, respectively, by the following convolutions:

$$c^1 = [x * h_0] \downarrow 2, \quad d^1 = [x * h_1] \downarrow 2.$$

Note that for $j=2$ and $j=3$ we have

$$c^2 = [h_0 * c^1] \downarrow 2, \quad d^2 = [h_1 * c^1] \downarrow 2,$$
$$c^3 = [h_0 * c^2] \downarrow 2, \quad d^3 = [h_1 * c^2] \downarrow 2.$$

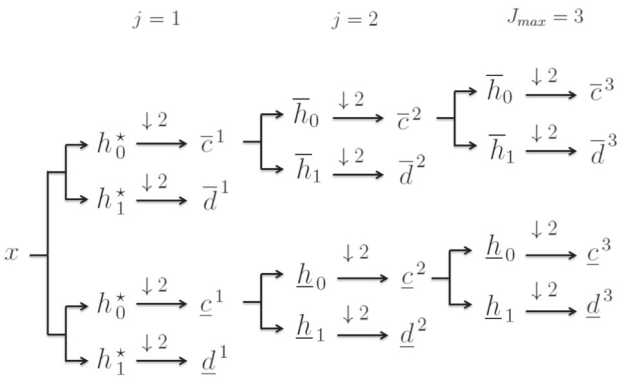

FIG. 14. Schematic multi-scale representation of three scales DT–CWT decomposition of the real time series x in three levels, where the filters $h_0^\star$ and $h_1^\star$ are considered in the level $j=1$. In levels $j=2$ and $j=3$, the filters of the upper and lower tree are $\bar{h}_0$, $\bar{h}_1$ and $\underline{h}_0$, $\underline{h}_1$, respectively.

APPENDIX C: DT–CWT DECOMPOSITION

A schematic representation of the DT-CWT decomposition is illustrated in Fig. 14. The real time series x is decomposed in $J_{max}=3$ scales, i.e., $j=1$, $j=2$, $j=3$, and the notation * is included in the first scale filters, i.e., $h_0^\star$ and $h_1^\star$.

In Ref. 49, it is shown that the implementation of the DT–CWT requires that the first scale of the dual-tree filter bank be different from the succeeding scales. A schematic representation of the DT–CWT decomposition is illustrated in Fig. 14. The real time series x is decomposed in $J_{max}=3$ scales, i.e., $j=1$, 2 and 3, and the notation * is included in the first scale filters, i.e., $h_0^\star$ and $h_1^\star$.

TABLE I. Non-zero near-symmetric (13, 19) and Q-Shift (14, 14)-tap filter coefficients. Credits N. G. Kingsbury, Appl. Comput. Harmonic Anal. **10**, 234–253 (2001). The coefficients are multiplied by 10^{-2}.

			Q-shift			
	Near-symmetric		Upper tree		Lower tree	
n	$h_0^\star$	$h_1^\star$	$\bar{h}_0$	$\bar{h}_1$	$\underline{h}_0$	$\underline{h}_1$
1	−0.17578	-7.0626×10^{-5}	0.32531	−0.45569	−0.45569	−0.32531
2	0	0	−0.38832	0.54395	−0.54395	−0.38832
3	2.22660	0.13419	3.46600	1.70250	1.70250	−3.46600
4	−4.68750	−0.18834	−3.88730	−2.38250	2.38250	−3.88730
5	−4.82420	−0.71568	−11.72000	−10.67100	−10.67100	11.72000
6	29.68800	2.38560	27.53000	−1.18660	1.18660	27.53000
7	55.54700	5.56430	75.61500	56.88100	56.88100	−75.61500
8	29.68800	−5.16880	56.88100	−75.61500	75.61500	56.88100
9	−4.82420	−29.9760	1.18660	27.53000	27.53000	−1.18660
10	−4.68750	55.9430	−10.67100	11.72000	−11.72000	−10.67100
11	2.22660	−29.9760	2.38250	−3.88730	−3.88730	−2.38250
12	0	−5.16880	1.70250	−3.46600	3.46600	1.70250
13	−0.17578	5.56430	−0.54395	−0.38832	−0.38832	0.54395
14		2.38560	−0.45569	−0.32531	0.32531	−0.45569
15		−0.71568				
16		−0.18834				
17		0.13419				
18		0				
19		-7.0626×10^{-5}				

APPENDIX D: DUAL-TREE FILTERS

In this work, we have chosen the Q-shift (14, 14) tap-filters where scales $j > 1$, which has provided a group delay of either $1/4$ or $3/4$ of a sample period, while also satisfying the usual 2-band filterbank constraints of no aliasing and perfect reconstruction.[71] For the first scale (13, 19) tap-filters were used, which are bi-orthogonal and near symmetric.

Table I presents the analysis filters coefficients used in this work.

[1]M. G. Rosenblum, A. S. Pikovsky, and J. Kurths, "Phase synchronization of chaotic oscillators," Phys. Rev. Lett. **76**, 1804–1807 (1996).
[2]M. G. Rosenblum, A. S. Pikovsky, and J. Kurths, "From phase to lag synchronization in coupled chaotic oscillators," Phys. Rev. Lett. **78**, 4193–4196 (1997).
[3]M. G. Rosenblum, A. S. Pikovsky, J. Kurths, C. Schäfer, and P. A. Tass, "Phase synchronization: From theory to data analysis," in *Handbook of Biological Physics* (Elsevier, New York, 2001), Vol. 4, pp. 279–321.
[4]M. G. Rosenblum, A. S. Pikovsky, J. Kurths, G. V. Osipov, I. Z. Kiss, and J. L. Hudson, "Locking-based frequency measurement and synchronization of chaotic oscillators with complex dynamics," Phys. Rev. Lett. **89**, 264102 (2002).
[5]A. S. Pikovsky, M. G. Rosenblum, and J. Kurths, *Synchronization: A Universal Concept in Nonlinear Sciences* (Cambridge, New York, 2003).
[6]B. Blasius and L. Stone, "Chaos and phase synchronization in ecological systems," Int. J. Bifurcation Chaos **10**, 2361–2380 (2000).
[7]J. Fell and N. Axmacher, "The role of phase synchronization in memory processes," Nat. Rev. Neurosci. **12**, 105–118 (2011).
[8]M. L. V. Quyen, J. Foucher, J. P. Lachaux, E. Rodriguez, A. Lutz, J. Martinerie, and F. J. Varela, "Comparison of Hilbert transform and wavelet methods for the analysis of neuronal synchrony," J. Neurosci. Methods **111**, 83–98 (2001).
[9]E. Lauro, S. Martino, M. Falanga, and S. Petrosino, "Synchronization between tides and sustained oscillations of the hydrothermal system of campi flegrei (Italy)," Geochem. Geophys. Geosyst. **14**, 2628–2637 (2013).
[10]I. Z. Kiss and J. L. Hudson, "Phase synchronization of nonidentical chaotic electrochemical oscillators," Phys. Chem. Chem. Phys. **4**, 2638–2647 (2002).
[11]M. Nixon, M. Friedman, E. Ronen, A. A. Friesem, N. Davidson, and I. Kanter, "Synchronized cluster formation in coupled laser networks," Phys. Rev. Lett. **106**, 223901 (2011).
[12]E. Rosa, C. M. Ticos, W. B. Pardo, J. A. Walkenstein, M. Monti, and J. Kurths, "Experimental Chua-plasma phase synchronization of chaos," Phys. Rev. E: Stat. Nonlinear Soft Matter Phys. **68**, 025202 (2003).
[13]E. Rosa, C. M. Ticos, W. B. Pardo, J. A. Walkenstein, M. Monti, and J. Kurths, "Phase synchronization in a plasma discharge driven by a chaotic signal," AIP Conf. Proc. **676**, 301–306 (2003).
[14]A. Bandrivskyy, A. Bernjak, P. McClintock, and A. Stefanovska, "Wavelet phase coherence analysis: Application to skin temperature and blood flow," Cardiovasc. Eng. **4**, 89–93 (2004).
[15]F. Mormann, K. Lehnertz, P. David, and C. E. Elger, "Mean phase coherence as a measure for phase synchronization and its application to the eeg of epilepsy patients," Phys. D **144**, 358–369 (2000).
[16]C. Schäfer, M. G. Rosenblum, H. H. Abel, and J. Kurths, "Synchronization in the human cardiorespiratory system," Phys. Rev. E **60**, 857–870 (1999).
[17]S. H. Strogatz and I. Stewart, "Coupled oscillators and biological synchronization," Sci. Am. **269**, 102–109 (1993).
[18]M. G. Rosenblum, A. S. Pikovsky, and J. Kurths, "Synchronization approach to analysis of biological systems," Fluctuation Noise Lett. **4**, L53–L62 (2004).
[19]P. Tass, M. G. Rosenblum, J. Weule, J. Kurths, A. Pikovsky, J. Volkmann, A. Schnitzler, and H. J. Freund, "Detection of *n*:*m* phase locking from noisy data: Application to magnetoencephalography," Phys. Rev. Lett. **81**, 3291–3294 (1998).
[20]T. Pereira, M. S. Baptista, and J. Kurths, "Multi-time-scale synchronization and information processing in bursting neuron networks," Eur. Phys. J. Spec. Top. **146**, 155–168 (2007).
[21]A. Pikovsky, M. Rosenblum, and J. Kurths, "Phase synchronization in regular and chaotic systems," Int. J. Bifurcation Chaos **10**, 2291–2305 (1999).
[22]M. C. Romano, M. Thiel, J. Kurths, I. Z. Kiss, and J. L. Hudson, "Detection of synchronization for non-phase-coherent and non-stationary data," Europhys. Lett. **71**, 466 (2005).
[23]J. Kurths, M. C. Romano, M. Thiel, G. V. Osipov, M. V. Ivanchenko, I. Kiss, and J. L. Hudson, "Synchronization analysis of coupled noncoherent oscillators," Nonlinear Dyn. **44**, 135–149 (2006).
[24]T. Pereira, M. S. Baptista, and J. Kurths, "General framework for phase synchronization through localized sets," Phys. Rev. E **75**, 026216 (2007).
[25]H. Fujisaka, T. Yamada, G. Kinoshita, and T. Kono, "Chaotic phase synchronization and phase diffusion," Phys. D **205**, 41–47 (2005).
[26]C. Kim, K. Kumar, B. Raj, and R. M. Stern, "Signal separation for robust speech recognition based on phase difference information obtained in the frequency domain," in *INTERSPEECH* (2009), pp. 2495–2498.
[27]A. Tyrrell and G. Auer, "Biologically inspired intercellular slot synchronization," J. Wireless Commun. Networking **2009**, Art. No. 12, 854087 (2009).
[28]T. Pereira, M. Baptista, and J. Kurths, "Phase and average period of chaotic oscillators," Phys. Lett. A **362**, 159–165 (2007).
[29]A. Balanov, N. Janson, D. Postnov, and O. Sosnovtseva, *Synchronization: From Simple to Complex* (Springer, New York, 2008).
[30]R. Follmann, E. E. N. Macau, and E. Rosa, "Detecting phase synchronization between coupled non-phase-coherent oscillators," Phys. Lett. A **373**, 2146–2153 (2009).
[31]R. Follmann, E. E. N. Macau, and E. Rosa, "Phase detection of chaos," Phys. Rev. E **83**, 016209 (2011).
[32]A. E. Hramov and A. A. Koronovskii, "An approach to chaotic synchronization," Chaos **14**, 603–610 (2004).
[33]A. E. Hramov, A. A. Koronovskii, and Y. Levin, "Synchronization of chaotic oscillator time scales," J. Exp. Theor. Phys. **100**, 784–794 (2005).
[34]A. E. Hramov and A. A. Koronovskii, "Time scale synchronization of chaotic oscillators," Phys. D **206**, 252–264 (2005).
[35]A. E. Hramov, A. A. Koronovskii, V. I. Ponomarenko, and M. D. Prokhorov, "Detection of synchronization from univariate data using wavelet transform," Phys. Rev. E **75**, 056207 (2007).
[36]A. A. Koronovskii and A. E. Hramov, "Chaotic phase synchronization studied by means of continuous wavelet transform," Tech. Phys. Lett. **30**, 587–590 (2004).
[37]A. A. Koronovskii and A. E. Hramov, "Wavelet transform analysis of the chaotic synchronization of dynamical systems," JETP Lett. **79**, 316–319 (2004).
[38]A. A. Koronovskii, M. Kurovskaya, and A. E. Hramov, "Relationship between phase synchronization of chaotic oscillators and time scale synchronization," Tech. Phys. Lett. **31**, 847–850 (2005).
[39]A. A. Koronovskii, V. I. Ponomarenko, M. D. Prokhorov, and A. E. Hramov, "Diagnostics of the synchronization of self-oscillatory systems by an external force with varying frequency with the use of wavelet analysis," J. Commun. Technol. Electron. **52**, 544–554 (2007).
[40]E. B. Postnikov, "On precision of wavelet phase synchronization of chaotic systems," J. Exp. Theor. Phys. **105**, 652–654 (2007).
[41]E. B. Postnikov, "Wavelet phase synchronization and chaoticity," Phys. Rev. E **80**, 057201 (2009).
[42]R. Q. Quiroga, A. Kraskov, T. Kreuz, and P. Grassberger, "Performance of different synchronization measures in real data: A case study on electroencephalographic signals," Phys. Rev. E **65**, 041903 (2002).
[43]I. Daubechies, "The wavelet transform, time-frequency localization and signal analysis," IEEE Trans. Inf. Theory **36**, 961–1005 (1990).
[44]N. G. Kingsbury, "The dual-tree complex wavelet transform: A new efficient tool for image restoration and enhancement," in *EUSIPCO* (1998), pp. 319–322.
[45]N. G. Kingsbury, "Shift invariant properties of the dual-tree complex wavelet transform," in *ICASSP* (1999), pp. 1221–1224.
[46]N. G. Kingsbury, "Image processing with complex wavelets," Philos. Trans. R. Soc. London, Ser. A **357**, 2543–2560 (1999).
[47]N. G. Kingsbury, "A dual-tree complex wavelet transform with improved orthogonality and symmetry properties," Int. Conf. Image Process. **2**, 375–378 (2000).
[48]N. G. Kingsbury, "Complex wavelets for shift invariant analysis and filtering of signals," Appl. Comput. Harmonic Anal. **10**, 234–253 (2001).
[49]I. W. Selesnick, R. G. Baraniuk, and N. G. Kingsbury, "The dual-tree complex wavelet transform," IEEE Signal Process. Mag. **22**, 123–151 (2005).
[50]E. E. N. Macau, C. Grebogi, and Y.-C. Lai, "Active synchronization in nonhyperbolic hyperchaotic systems," Phys. Rev. E **65**, 027202 (2002).

[51]I. Daubechies, J. Lu, and H. T. Wu, "Synchrosqueezed wavelet transforms: An empirical mode decomposition-like tool," Appl. Comput. Harmonic Anal. **30**, 243–261 (2011).
[52]D. Iatsenko, A. Bernjak, T. Stankovski, Y. Shiogai, P. J. Owen-Lynch, P. Clarkson, P. McClintock, and A. Stefanovska, "Evolution of cardiorespiratory interactions with age," Philos. Trans. R. Soc. London, Ser. A **373**, 1–18 (2013).
[53]G. Thakur, E. Brevdo, N. S. Fuckar, and H.-T. Wu, "The synchrosqueezing algorithm for time-varying spectral analysis: Robustness properties and new paleoclimate applications," Signal Process. **93**, 1079–1094 (2013).
[54]H. T. Wu, Y. H. Chan, Y. T. Lin, and Y. H. Yeh, "Using synchrosqueezing transform to discover breathing dynamics from ecg signals," Appl. Comput. Harmonic Anal. **36**, 354–359 (2014).
[55]B. Kralemann, M. Frühwirth, A. Pikovsky, M. Rosenblum, T. Kenner, J. Schaefer, and M. Moser, "*In vivo* cardiac phase response curve elucidates human respiratory heart rate variability," Nat. Commun. **4**, 2418 (2013).
[56]B. Kralemann, L. Cimponeriu, M. Rosenblum, A. Pikovsky, and R. Mrowka, "Phase dynamics of coupled oscillators reconstructed from data," Phys. Rev. E **77**, 066205 (2008).
[57]J. T. C. Schwabedal, A. Pikovsky, B. Kralemann, and M. Rosenblum, "Optimal phase description of chaotic oscillators," Phys. Rev. E **85**, 026216 (2012).
[58]J. P. Lachaux, E. Rodriguez, J. Martinerie, and F. J. Varela, "Measuring phase synchrony in brain signals," Hum. Brain Mapp. **8**, 194–208 (1999).
[59]L. W. Sheppard, A. Stefanovska, and P. V. E. McClintock, "Testing for time-localized coherence in bivariate data," Phys. Rev. E **85**, 046205 (2012).
[60]A. V. Tankanag, A. A. Grinevich, T. V. Kirilina, G. V. Krasnikov, G. M. Piskunova, and N. K. Chemeris, "Wavelet phase coherence analysis of the skin blood flow oscillations in human," Microvasc. Res. **95**, 53–59 (2014).
[61]Y. Kuramoto, "Self-entrainment of a population of coupled non-linear oscillators," *International Symposium on Mathematical Problems in Theoretical Physics* (1975), Vol. 39, pp. 420–422.
[62]R. L. Burden and J. D. Faires, *Numerical Analysis* (Brooks Cole, Belmont, MA, 2010).
[63]W. Kühnel, *Diffferential Geometry: Curves, Surfaces, Manifolds*, Europe and Central Asia Environmentally and Socially Sustain (American Mathematical Society, Providence, 2002).
[64]M. W. Hirsch, S. Smale, and R. L. Devaney, *Differential Equations, Dynamical Systems, and an Introduction to Chaos* (Elsevier, New York, 2004), Vol. 60.
[65]O. E. Rössler, "An equation for continuous chaos," Phys. Lett. A **57**, 397–398 (1976).
[66]K. Alligood, T. Sauer, and J. Yorke, *Chaos: An Introduction to Dynamical Systems* (Springer, New York, NY, 1997).
[67]S. Boccaletti, J. Kurths, G. Osipov, D. Valladares, and C. Zhou, "The synchronization of chaotic systems," Phys. Rep. **366**, 1–101 (2002).
[68]J. Y. Chen, K. W. Wong, and J. W. Shuai, "Properties of phase locking with weak phase-coherent attractors," Phys. Lett. A **285**, 312–318 (2001).
[69]S. G. Mallat, *A Wavelet Tour of Signal Processing* (Academic Press, New York, 1998).
[70]S. G. Mallat, "A theory for multiresolution signal decomposition: The wavelet representation," IEEE Trans. Pattern Anal. Mach. Intell. **11**, 674–693 (1989).
[71]N. G. Kingsbury, "Design of q-shift complex wavelets for image processing using frequency domain energy minimization," Int. Conf. Image Process. **1**, I-1013-16 (2003).